

Article

The On-Line Identification and Location of Welding Interference Based on CEEMD

Peng Yu ^{1,2}, Haichao Song ^{1,2}, Yukuo Tian ³, Juan Dong ⁴, Guocheng Xu ⁴, Mingming Zhao ⁵ and Xiaopeng Gu ^{4,*} 

¹ Engineering Technology Training Center, Nanjing Vocational University of Industry Technology, Yangshan North Rd. 1, Nanjing 210023, China; 2020101125@niit.edu.cn (P.Y.); songhc@niit.edu.cn (H.S.)

² Jiangsu Province Precision Manufacturing Engineering and Technology Research Center, Nanjing 210023, China

³ Zhejiang Academy of Special Equipment Science, Kaixuan Str. 211, Hangzhou 310020, China; tianyukuo@163.com

⁴ Department of Materials Science and Engineering, Jilin University, Renmin Str. 5988, Changchun 130025, China; dongjuan@jlu.edu.cn (J.D.); xgc@jlu.edu.cn (G.X.)

⁵ Xuzhou Construction Machinery Group Truck-Mounted Crane Co., Ltd., Tuolan Rd. 55, Xuzhou 221004, China; 18652212532@163.com

* Correspondence: guxp@jlu.edu.cn

Abstract: The welding process itself is a non-linear, multivariable, coupled physical metallurgical process that is easily perturbed. Improper welding parameter selection and welding process conditions will interfere with the welding process and affect the final welding quality. This study aims to identify and locate two types of welding interference, insufficient shielding gas and unremoved oxidation film on the base metal surface, during the Pulse Multi-Control Gas Metal Arc Welding (PMC GMAW) process of aluminum alloy. The Characteristic Intrinsic Mode Function (IMF), which is closely related to the short circuit transition process, was obtained by applying the Complementary Ensemble Empirical Mode Decomposition (CEEMD) method to the welding current signal measured during the welding process. Time and frequency domain analysis of the acquired characteristic IMF was then performed. The experimental results demonstrated that for a stable welding process, the frequency of the characteristic IMF is concentrated within a narrow range. The frequency spectrum of the characteristic IMF exhibits distinct variations under different types of welding interference. Based on this, the chronological arrangement of characteristic IMF components' frequency spectrum allows for locating welding interferences by analyzing their abnormal signals within the reconstructed signal sequence.

Keywords: on-line monitoring; CEEMD; time-frequency analysis; feature extraction; welding current waveform



Citation: Yu, P.; Song, H.; Tian, Y.; Dong, J.; Xu, G.; Zhao, M.; Gu, X. The On-Line Identification and Location of Welding Interference Based on CEEMD. *Metals* **2024**, *14*, 396. <https://doi.org/10.3390/met14040396>

Academic Editors: Frank Czerwinski and Masahiro Fukumoto

Received: 20 February 2024

Revised: 17 March 2024

Accepted: 26 March 2024

Published: 28 March 2024



Copyright: © 2024 by the authors. Licensee MDPI, Basel, Switzerland. This article is an open access article distributed under the terms and conditions of the Creative Commons Attribution (CC BY) license (<https://creativecommons.org/licenses/by/4.0/>).

1. Introduction

Aluminum alloy is an ideal material for achieving lightweight manufacturing, owing to its high strength, low density, and corrosion resistance. Consequently, it has gained extensive utilization in the fields of shipbuilding, automotive engineering, aerospace technology, and machinery production. The accurate and consistent control of real-time heat input adjustments is a challenge due to the high sensitivity of aluminum alloys to heat input. In addition, the welding process itself is a dynamic non-linear, multivariable, coupled physical metallurgical process that is highly susceptible to environmental disturbances. Numerous factors influence the stability of the welding process, and the improper selection of welding parameters and conditions can disrupt the welding process and impact the final weld quality. On-line weld-quality monitoring of the aluminum alloy welding process is challenging.

Welding process signals such as welding electrical signals (welding voltage and current), molten pool vision signals, arc acoustic signals, and arc spectral signals are closely

related to the droplet transfer mode, arc shape, and welding process stability. Extracting valuable characteristic information from welding process signals is a critical issue in welding monitoring. In recent years, a number of studies have been carried out in order to develop a method by which the measured signal characteristics can be used for the on-line identification of weld defects [1,2]. Zhang et al. developed a monitoring system for robotic GTAW using a spectrometer, charge-coupled device camera, and microphone for the on-line detection of inner porosity [3]. Gao et al. developed a high-speed imaging system for the on-line monitoring of the welding process. The system can simultaneously obtain visual information from the top and bottom of the weld. Based on the visual characteristics, multiphysical phenomena such as droplet transfer and keyhole status have been successfully quantified [4,5]. Zhang et al. acquired the Acoustic Emission (AE) and air-coupled Ultrasonic Testing (UT) signal for on-line monitoring of the welding process, especially for burn-through [6]. Jin developed a method using a Deep Neural Network (DNN) to monitor the weld gap and control the weld deposition rate, thereby automating the hull block welding process. The average accuracy for off-line and on-line cases was 93.7% and 87.7%, respectively [7]. An innovative approach proposed by Huang et al. involves the analysis of spectral data obtained during the welding process of aluminum alloys to diagnose and detect porosity defects. The classification accuracy of their improved Support Vector Machine (SVM) classification model reached up to 92.5% [8].

Compared to other welding process signals, the welding voltage and current signals have strong anti-interference ability and can accurately reflect the real-time change of the arc in the welding process. The magnitude and waveforms of the welding current had a significant effect on the heat input, weld bead shape, and pool behavior, as the welding current determines the arc force, heat input, and pool viscosity [9,10]. In addition, welding voltage and current sensors offer advantages over other sensing devices such as their low cost, relatively simple structure, compact size, easy installation, and independence from both the welding environment and station limitations. These advantages have led to the widespread use of monitoring equipment and methods based on welding electrical signals in practical production. Jin et al. utilized scalogram feature image data extracted from the welding current signal to develop labeled weld quality training data for a convolutional neural network model, which was employed for monitoring and predicting back-bead generation. The average prediction accuracy of their model was around 93.5% [11]. Zhao et al. measured the welding current and voltage signal to obtain the power signal. They extracted five characteristics from the power signal to characterize the welding quality [12]. Huang et al. decomposed the current signal into a series of IMFs and utilized the energy entropy and normalized energy as a feature vector for weld quality classification [13].

Our previous studies focused on the on-line monitoring of welding stability and real-time identification of geometric defects, including undercutting, humping, and the lack of fusion [14]. The presence of hydrogen porosity in the weld will greatly reduce the strength of the weld. The two main factors contributing to the formation of hydrogen porosity in aluminum alloy welds are the insufficient flow of protective gas and the presence of oxidation film on the surface of the aluminum alloy. In this paper, the above two factors were employed to disturb the welding process, and the welding current signal during the PMC GMAW process was measured using a Hall sensor. The CEEMD method was employed to decompose the recorded welding current signal. Then, the original measured data and a series of intrinsic mode functions were compared and analyzed in the time-frequency domain, and the IMF closely associated with the short-circuit transfer process was selected as the characteristic IMF. The welding interference can be qualitatively identified and located based on the frequency spectrum distribution features of the characteristic IMF.

2. Experiment Setup

Automated GMAW was carried out using a manufactured TPS-500i (Fronius, Wels, Austria) power supply, and a single-pass weld was performed to form a butt weld without a groove. Figure 1 shows the welding current waveform of the PMC GMAW process, and

the droplet transition process is divided into two steps. During the first pulse period, an arc is generated between the tip of the welding wire and the base material, resulting in the gradual melting of the tip of the welding wire and the subsequent formation of a molten metal droplet. In this step, the welding current exhibits a relatively higher value while the welding wire moves towards the molten pool, gradually reducing the distance between the tip of the welding wire and the molten pool. The arc is then extinguished as soon as contact is made between the molten droplet and the molten pool. During the following two pulse periods, surface tension, electromagnetic pinch force, and gravity act on the liquid bridge, causing the droplet to grow and fall apart. The characteristic feature of this process is the minimal increase in short-circuit current at the point of contact between the droplet and the pool, as the welding power supply automatically reduces the welding current. In comparison to conventional pulsed arc welding processes, this technique effectively reduces the overall heat input during welding, mitigates excessive spatter, and improves both arc stability and overall weld quality.

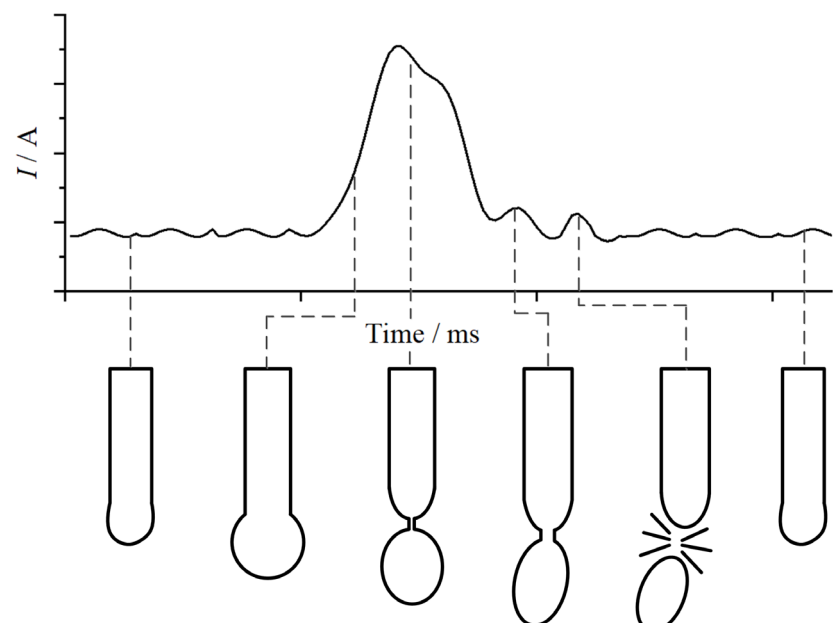


Figure 1. The welding current waveform in PMC GMAW.

A synergistic program automatically adjusts the welding voltage, wire feed speed, and wire movement based on the welding current. In general, for a given set of welding conditions (e.g., wire diameter and composition, wire feed speed, etc.), there are many welding parameters that can achieve a stable welding process, and the rational combination of welding parameters can be selected to best meet other requirements specific to the particular application. After many trials, the authors have made several modifications to the recommended welding parameters given by the welding supply company in order to achieve the best weld formation and low weld spatter. The welding parameters that are set on the power source are listed in Table 1. In order to improve the protection of the arc and the pool of molten metal, a diversion mesh (filter net) has been installed inside the welding torch. The welding current data generated in the experiment were collected using a Hall sensor at a sampling rate of 10 kHz. The Hall sensor has a current measurement range of 0–1000 A and a rated output voltage of $4 \pm 1\%$ V. The measured current signal was transmitted to an industrial computer via a 10-bit multifunction data acquisition card.

The arc and molten pool were shielded from oxidation during the experiment by employing argon with a level of 99.95% purity. The scale of the 6082 aluminum alloy base material is 200 mm (length) \times 100 mm (width) \times 4 mm (thickness), and the 5087 aluminum alloy is used as the welding wire ($\Phi 1.2$ mm). The welding torch was pointed at 45 degrees to the welding direction. The polished plates were brushed with a steel brush to remove

oxide layers before being positioned and clamped down on the welding table. The chemical composition of the base metal and welding wire are given in Table 2.

Table 1. Welding parameters.

Trial Number	Welding Current I/A	Welding Voltage U/V	Welding Speed V/mm·s ⁻¹	Shielding Gas Flow Rate V ₁ /L·min ⁻¹	Base Metal Surface Condition
1					polished
2				25	unpolished
3	175	21.4	10		first half polished second half unpolished
4				10	polished
5				first half 25 second half 10	polished

Table 2. Chemical compositions of base metal and filler wire metal (nominal values).

Al Alloy Series	Si	Fe	Cu	Mn	Mg	Cr	Zn	Ti	Zr	Al
6082	0.79	0.50	0.10	0.58	0.96	0.25	0.20	0.10	0.00	96.52
5087	0.25	0.40	0.05	0.81	4.60	0.10	0.25	0.15	0.13	93.26

3. Method

Empirical Mode Decomposition (EMD) is an adaptive time-frequency signal processing method that is intended for non-linear and non-stationary signals [15]. This decomposition method is an intuitive, direct, and adaptive method which is based on and derived only from signal data. This method decomposes the input signal into a set of Intrinsic Mode Functions (IMFs) based on the inherent characteristics of the signal. However, due to the problem of mode mixing, the input signal cannot be accurately decomposed when the EMD method is applied to non-stationary signals containing intermittent signal components.

To solve the disadvantage of mode mixing, Wu and Huang developed Ensemble Empirical Mode Decomposition (EEMD) to improve the effectiveness of EMD [16]. By adding Gaussian white noise into the input signal and calculating the means of the IMFs repeatedly, the EEMD method increases the accuracy and efficiency of signal decomposition. The addition of white noise improves the spectral composition of the signal across the entire spectrum, thereby reducing mode mixing. Although the EEMD method effectively prevents mode mixing, it is time-consuming to implement a sufficiently large ensemble mean; that is to say, the algorithm efficiency will be greatly reduced.

To address this issue, the complementary ensemble EMD (CEEMD) method is proposed [17]. In contrast to EEMD, CEEMD involves the extraction of residual white noise from mixtures of data and white noise using pairs of complementary ensemble IMFs containing positive and negative added white noise. The performance of the CEEMD method is comparable to that of the EEMD method, with a significant increase in computational efficiency. The CEEMD method has been widely used for feature extraction and fault detection in recent years [18–21]. The mathematical description of the CEEMD is included in this paper [17].

The procedure for the implementation of the CEEMD is shown below:

- (1) Add two reverse white noises to input signal $x(t)$:

$$m_i^+(t) = x(t) + n_i^+, \quad (1)$$

$$m_i^-(t) = x(t) + n_i^-. \quad (2)$$

- (2) Decompose $m_i^+(t)$ and $m_i^-(t)$ by the EMD method.
- (3) Calculate the ensemble mean of the corresponding imf generated from each trial IMF 1 and IMF 2.

- (4) Calculate the average of IMF 1 and IMF 2 as the final decomposition result:

$$IMF = \frac{(IMF1 + IMF2)}{2}. \quad (3)$$

The flow chart of CEEMD is shown in Figure 2, where n is the decomposition trials.

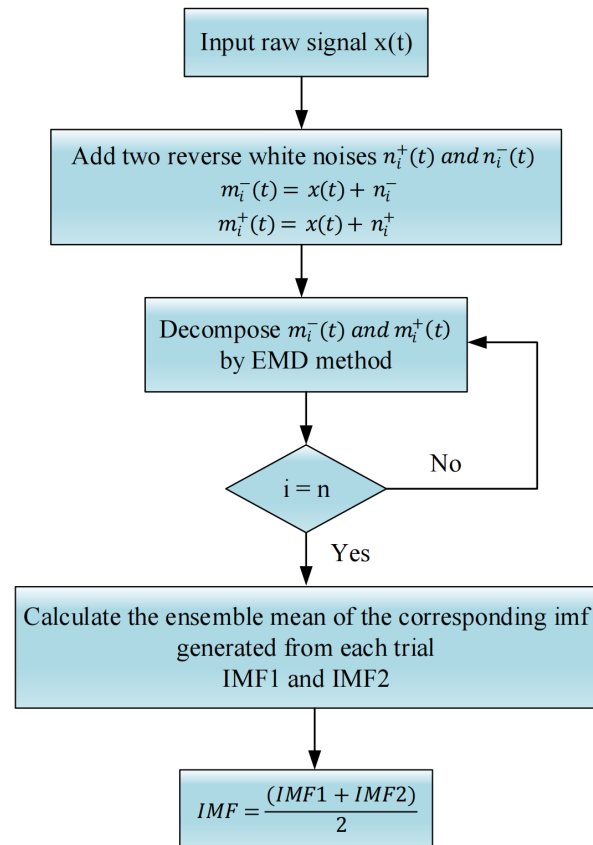


Figure 2. The flow chart of CEEMD.

4. Results and Discussion

4.1. Extraction the Characteristic IMF

During the PMC GMAW process, variations in the waveform of the welding current correspond to different stages of short-circuit transfer. For a stable welding process, the welding current signal should be a periodic reproduction of the welding current waveform. As shown in Figure 3, the waveform of the welding current signal generated throughout the entire welding process remained almost unchanged, and the waveform characteristic parameters such as amplitude, phase, and frequency fluctuated within a small range.

The partial welding current waveforms (0.1 s) collected in real time during trial 1 are depicted in Figure 3. It can be observed from the figure that the unfiltered signal contains significant noise. To facilitate analysis in the frequency domain, the original signal is first filtered using a type I Chebyshev filter. Considering that the pulse frequency of MIG welding current signals is typically in the range of 20 to 200 Hz, a bandpass frequency range of 10 to 300 Hz was set. Figure 3 illustrates that the welding current signal waveform during each short-circuit transfer period in the PMC welding process exhibits a remarkable similarity, characterized by a high-amplitude pulse followed by two low-amplitude pulses. When setting the welding current to 175 A, approximately 20 complete short circuit transition cycles occur within a 100 ms interval, indicating an average duration of approximately 5 ms for each short circuit transition cycle and a corresponding frequency of about 200 Hz.

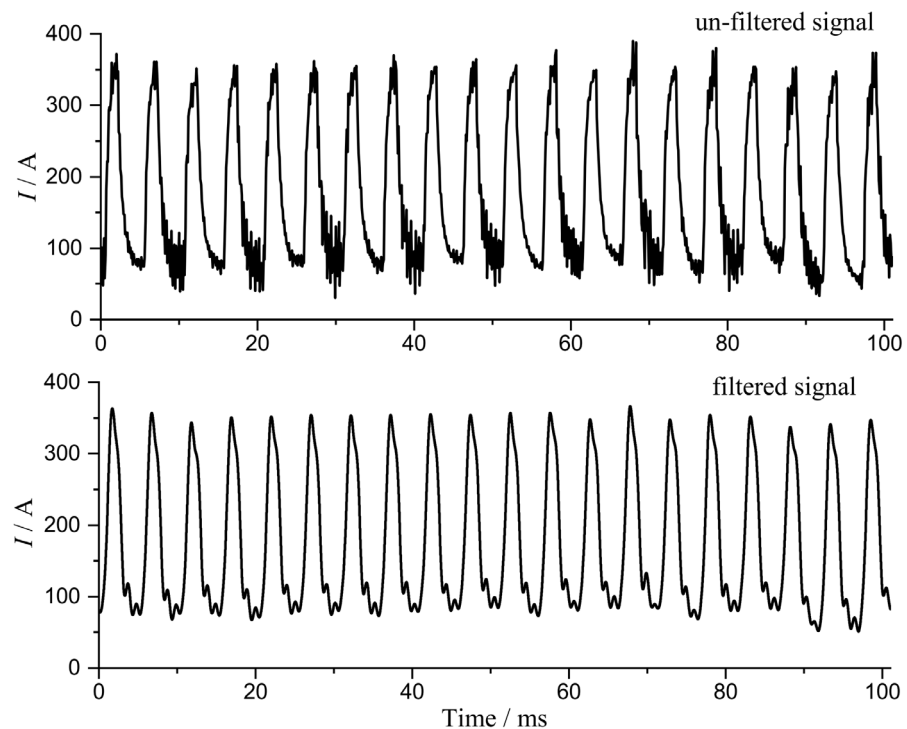


Figure 3. Welding current signal of trial 1.

The welding current signal generated during the welding process is a typical non-stationary signal. To obtain further information in the frequency domain, the filtered welding current signal shown in Figure 3 is decomposed using the CEEMD method. A series of IMFs are then transformed using Fast Fourier Transform (FFT) and sorted from high to low based on their frequencies, as shown in Figure 4.

The first six IMF components obtained after decomposition and their frequency spectrum are illustrated in Figure 4. It can be observed from Figure 4b,d that both IMF 1 and IMF 2 exhibit a dominant frequency higher than 1000 Hz with relatively small signal amplitudes. Therefore, the above components can be regarded as signal noise when analyzing the frequency domain characteristics of welding current signals. Compared to the welding current signal shown in Figure 3, IMF 5 and IMF 6 exhibit excessively low dominant frequencies, as shown in Figure 4j,l, and lack the typical characteristics of pulse signals. It can be observed from Figure 4e,g that both IMF 3 and IMF 4 display typical temporal characteristics of pulse signals, manifested by the repeated occurrence of periodic waveforms. By comparing the pulse signals in Figure 4e,g with the welding current signals in Figure 3, it can be seen that the pulse frequency of IMF 4 is similar to that of the original signal. In addition, the phase and change trend of each pulse in IMF 4 are identical to those of the original signal, providing a one-to-one correspondence in the time domain, and IMF 4 can, therefore, be considered as the characteristic IMF component closely related to the short-circuit transfer process. This component can well characterize the fluctuation of the original signal, i.e., the short-circuit transfer and the droplet transition in the welding.

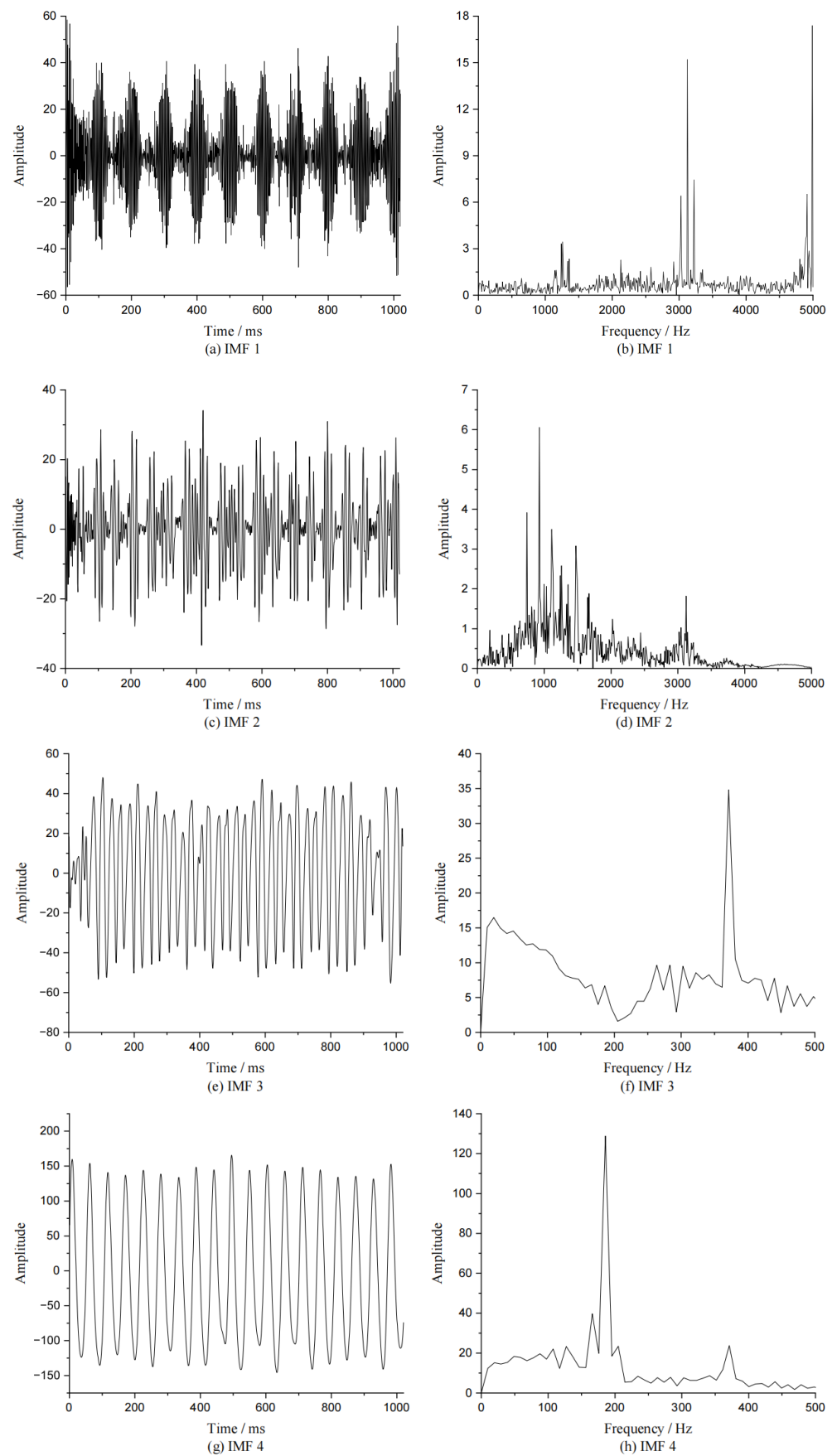


Figure 4. Cont.

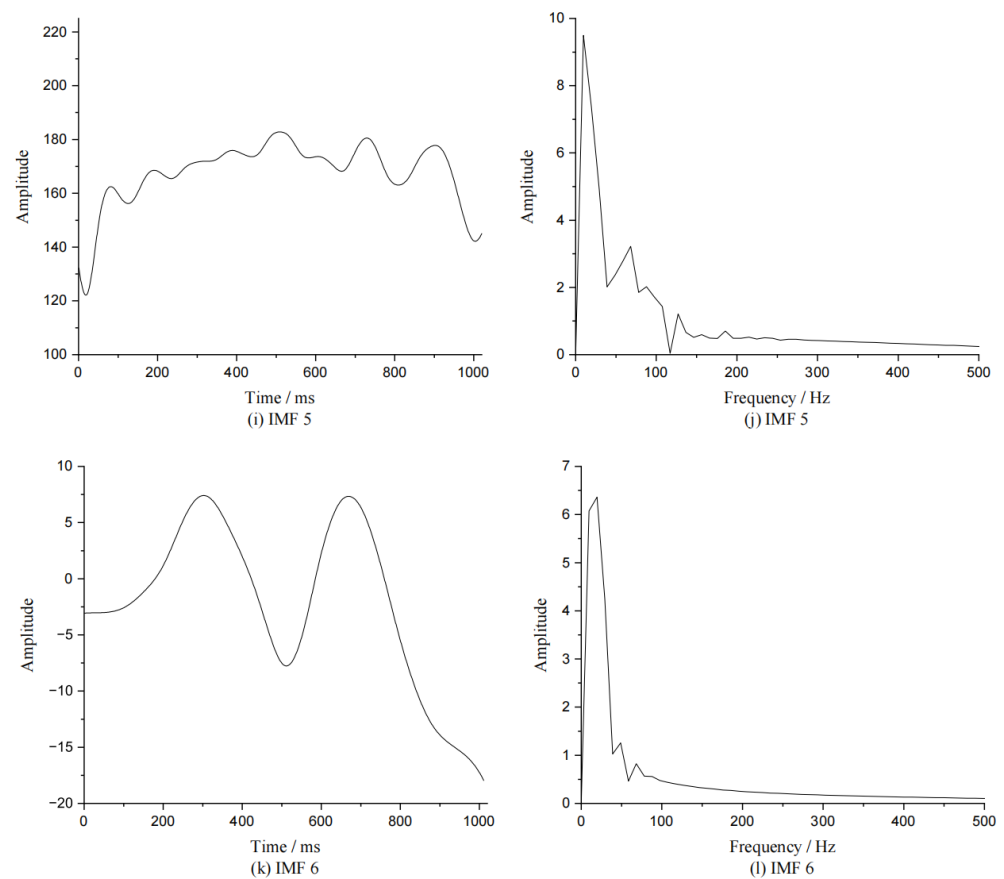
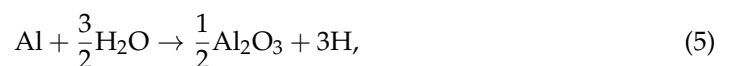


Figure 4. First six IMF components and corresponding frequency spectra of the welding current signal collected in trial 1.

4.2. Identification of Welding Inference

4.2.1. Surface with Oxidation Film

The presence of an oxidation film on the surface of the aluminum alloy has a significant effect on the weld quality of the joint and can easily cause porosity defects. The oxidation film has strong adsorption properties, allowing it to absorb moisture from the surrounding air. During the welding process, the liquid metal in the molten pool reacts with the water absorbed by the oxidation film, resulting in a significant generation of hydrogen gas. To be more specific, at high temperature, water can be directly decomposed to produce hydrogen and react with liquid aluminum in the molten pool to produce hydrogen. The chemical equations are shown in (4) and (5).



The solubility of hydrogen in liquid aluminum and solid aluminum is very different, so after hydrogen dissolves into the liquid metal within the molten pool, with the gradual cooling and solidification of the molten pool, hydrogen will precipitate a large number of bubbles, and these bubbles will form hydrogen pores in the weld if they cannot escape in time. Therefore, the removal of any oxidation films present on the base metal surfaces is typically necessary for achieving high-quality welded joints during practical production processes.

As can be seen from Figure 5, when the base metal was welded with an oxidation film on its surface, the dominant frequency of the characteristic IMF decreased significantly compared to the stable welding process, from about 195 Hz to approximately 185 Hz. The

decrease in the dominant frequency indicates that the short-circuit transfer frequency of the welding process is decreasing. It is also clear from the figure that there is a significant increase in signal energy near the dominant frequency range, suggesting that the short-circuit transfer and the welding process are being disturbed. In comparison to the stable welding process, the difference can be used as the judgment of the base metal with oxidation film.

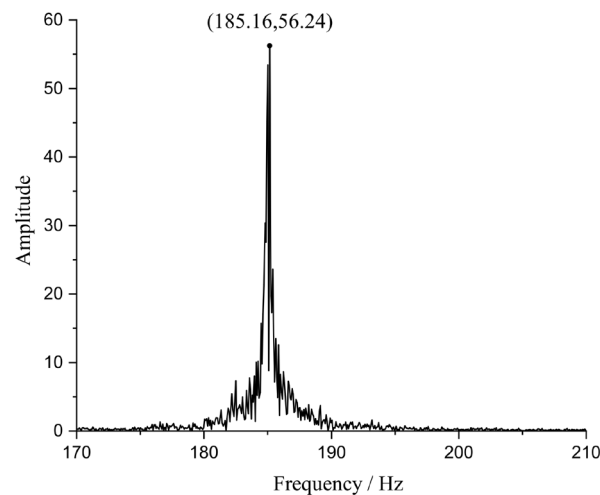


Figure 5. The frequency spectra of the characteristic IMF component of trial 2.

4.2.2. Insufficient Flow Rate of Shielding Gas

The inert gas acts as a protective barrier, effectively isolating the arc and molten pool from the ambient air and preventing any chemical reaction between the molten metal and the external environment. The significant reduction in shielding gas flow will result in inadequate protection of the arc, preventing the arc from maintaining continuous and stable combustion. This leads to instability in both the short-circuit process and droplet transition processes. The welding result, particularly the mechanical properties and microstructure of the aluminum alloy, can be influenced by both the flow rate and the purity of the argon gas [22].

In trial 4, the shielding gas flow rate was reduced to 10 L/min, while the other welding parameters remained unchanged. The welding current signal collected in trial 4 was decomposed using the CEEMD method, and the IMF 4 component was transformed by FFT. The frequency spectrum of the characteristic IMF component is illustrated in Figure 6. As depicted in the figure, compared to a stable welding process, as shown in Figure 4h, an insufficient flow rate of protective gas leads to significant changes in the frequency distribution of the characteristic IMF. There are two obvious peaks in the frequency spectrum, which have an M-shaped distribution, indicating that the short-circuit transfer process in the welding process does not occur at a fixed frequency. The peak was observed at around 192 Hz and 195 Hz. Furthermore, the valley between these two prominent peaks suggests rapid changes in the short-circuit transfer frequency. This abrupt frequency switching is responsible for the instability observed during the welding process. The characteristic IMF frequency spectrum of the stable welding process, as shown in Figure 4h, does not have the above characteristics, and welding interference, i.e., insufficient shielding gas flow, can be qualitatively identified from this difference.

Short-circuit frequency plays a critical role in determining the stability of the welding process. Time-frequency spectral analysis can effectively assess the stability and quality of GMAW [11]. From the analysis of the frequency spectrum of the characteristic IMF, it can be seen that the frequency distribution of the characteristic IMF extracted from the welding current signal is different under different welding conditions.

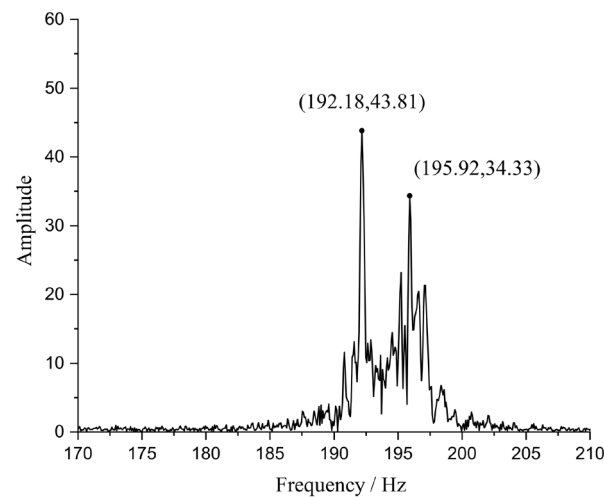


Figure 6. The frequency spectra of the characteristic IMF component of trial 4.

4.3. Location of Welding Inference

The uniformity of the droplet transition frequency is affected by the instability of the arc state during arc initiation and extinguishing. The presence of frequency information in these two stages can interfere with the final analysis results in the frequency domain. Therefore, before signal processing, the signals corresponding to the arcing and extinguishing phases are excluded from the original data of trials 1, 3, and 5. The welding current signal for the remaining 14 s was divided equally into 14 data fragments of equal length, which were then decomposed using CEEMD. Finally, the FFT was performed on all characteristic IMF components, and the frequency spectrum was arranged in time order. As shown in Figure 7, the x and y axes represent time and frequency, respectively, while the z axis represents the magnitude of the frequency.

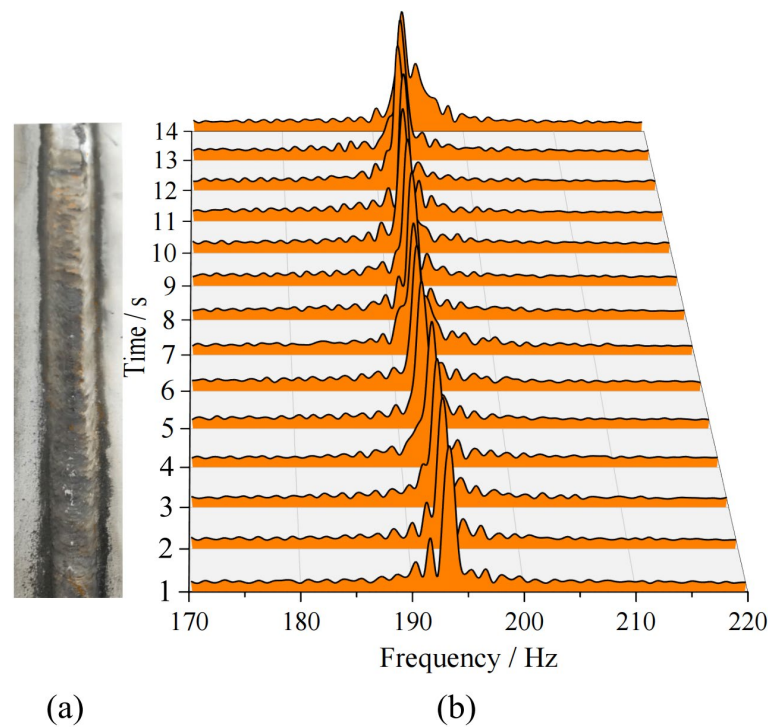


Figure 7. The frequency spectra of the characteristic IMF components of trial 1, (a) weld appearance. (b) frequency spectrum arranged in time order.

The weld in trial 1, as depicted in Figure 7a, was well formed, without any surface weld defects or spatter around the weld. Furthermore, as illustrated in Figure 7b, the frequency distribution of the 14 data fragments closely resembles the characteristic IMF frequency distribution observed during stable welding processes, as shown in Figure 4h. The dominant frequency distribution is within a narrow range, mainly concentrated in 194–195.5 Hz, indicating that the welding process parameters are properly selected and the welding process is relatively stable.

The frequency spectrum of the characteristic IMF components of trial 3 is depicted in Figure 8b. Notably, due to the presence of an unremoved oxidation film on the surface of the base metal, a peak with higher energy can be observed in the low-frequency region to the left of the dominant frequency at the 10th second. The frequency distribution exhibits significant deviation from the stable welding process. For the latter half of the welding process, there was a wide frequency distribution, and the highest frequency was close to 185 Hz in Figure 8b, indicating that the presence of the surface oxidation film increases the non-uniformity of the short-circuit transfer process.

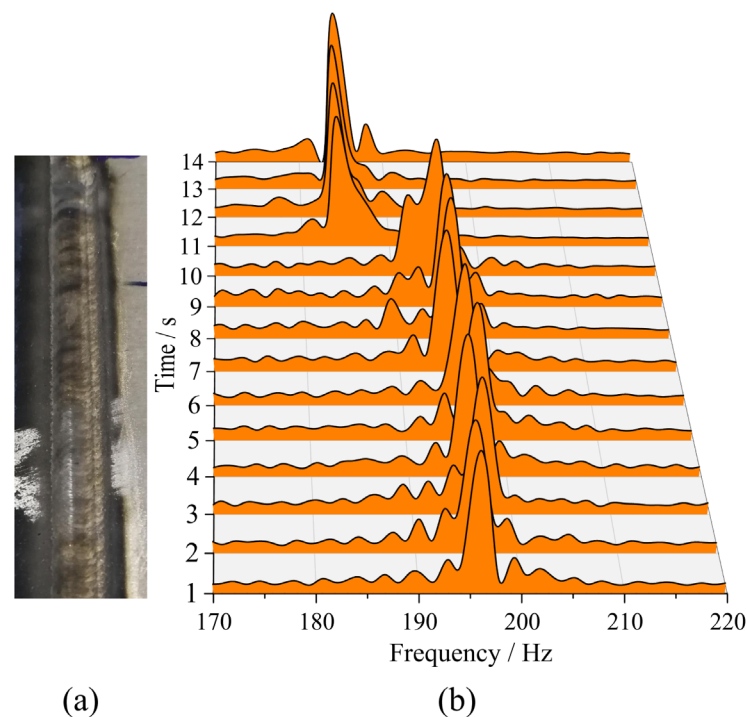


Figure 8. The frequency spectra of the characteristic IMF components of trial 3. (a) weld appearance. (b) frequency spectrum arranged in time order.

Figure 9b shows the change in the frequency spectrum of the characteristic IMF of trial 5 when the shielding gas is suddenly reduced during the welding process. It can be seen that during the first half of the welding process (1–7 s), the waveform is similar to Figure 4h, with a peak frequency at around 195 Hz and a narrow frequency energy distribution, indicating relative stability in the welding process. The shielding gas flow was abruptly reduced to 10 L/min at the 8th second, resulting in inadequate protection of the arc by argon gas in the latter half. As a result, there is a significant difference in the signal energy distribution compared to the first half of the welding process. As shown in Figure 9b, the signal amplitude decreased by between 9 s and 14 s, and there is a significant increase in signal energy over a relatively wide frequency range towards lower frequencies. This phenomenon can be attributed to the sudden reduction of shielding gas, leading to an unstable arc and short-circuiting process. In addition, during the welding process, part of the heat is removed by the shielding gas blown onto the base metal. During the first phase of welding (1–7 s), there exists a dynamic equilibrium between heat input and dissipation,

resulting in well-formed welds. However, starting from the 8th second, a sudden decrease in the flow rate of the protective gas significantly reduces the heat dissipation, resulting in localized melting on the back of the plate without any molten metal exiting and creating a gap between the plates. Two prominent peaks can be observed in the last six data fragments of Figure 9b. It is considered that the appearance of the new peak at around 192 Hz is closely related to the increase in arc length during the generation of the burn-through, as shown in Figure 9a. In the last six data fragments, the sudden change in the IMF frequency spectrum distribution is consistent with the change in weld morphology.

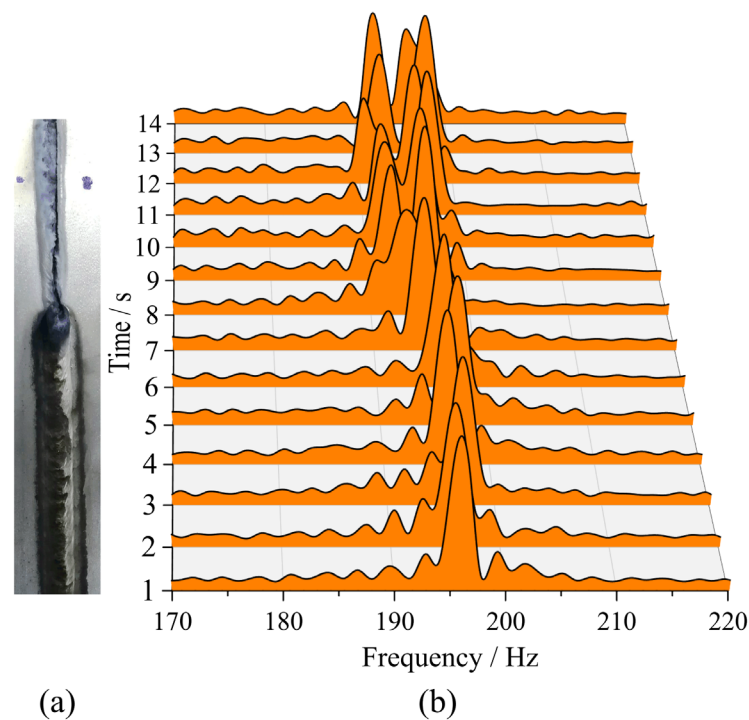


Figure 9. The frequency spectra of the characteristic IMF components of trial 5. (a) weld appearance. (b) frequency spectrum arranged in time order.

In particular, the frequency distribution of the last six data fragments is similar to that shown in Figure 6. Therefore, by employing the time-frequency analysis method based on the frequency distribution of the characteristic IMF, it becomes feasible to accurately detect and localize disturbances such as insufficient shielding gas and unremoved oxidation film on the base metal.

5. Conclusions

In this paper, the CEEMD method was used to decompose the welding current signal measured during the PMC GMAW process. The frequency spectrum of the characteristic IMF was analyzed in both time and frequency domains. The main conclusions are as follows:

1. For a stable welding process, the frequency of the characteristic IMF is concentrated within a narrow range, with a specific dominant frequency.
2. The CEEMD can successfully decompose the characteristic IMF, which is closely related to the short-circuit frequency from the welding current.
3. By analyzing the frequency spectrum of the characteristic IMF, disturbances such as insufficient shielding gas and the base metal surface with oxidation film can be identified and located.

The on-line welding interference identification and location method proposed in this study contribute to the automation of manufacturing; however, this study has certain

limitations. Therefore, in future research, we plan to focus on distinguishing between acceptable interferences and interferences that cause serious welding defects during the welding process in order to apply the proposed method in the actual manufacturing process. In addition, the influence of other variables on IMF and weld quality should be further investigated to improve the understanding of process kinetics.

Author Contributions: Conceptualization, P.Y. and Y.T.; methodology, J.D. and M.Z.; software, P.Y.; validation, P.Y. and X.G.; formal analysis, P.Y.; investigation, P.Y.; resources, X.G.; data curation, J.D. and M.Z.; writing—original draft preparation, H.S. and G.X.; writing—review and editing, X.G., P.Y. and Y.T.; visualization, P.Y. and X.G.; supervision, P.Y. and X.G.; project administration, P.Y. and X.G.; funding acquisition, H.S. and G.X. All authors have read and agreed to the published version of the manuscript.

Funding: This research was funded by the Jiangsu Province Precision Manufacturing Engineering and Technology Research Center, the Starting Research Fund of Nanjing Vocational University of Industry Technology (grant number YK20-14-06), the Jiangsu Provincial Modern Agricultural Machinery Equipment and Technology Demonstration Programs (grant number NJ2023-01, NJ2023-28), Regulated Research Projects of National Education Science (grant number C/2023/02/12), Independent Innovation of Agricultural Science and Technology of Jiangsu Province (grant number CX(22)3103), and the Jiangsu Provincial Double-Innovation Doctor Program (grant number JSSCB20210629).

Data Availability Statement: The data presented in this study are available on request from the corresponding author.

Conflicts of Interest: Author Mingming Zhao was employed by the company Xuzhou Construction Machinery Group Truck-Mounted Crane Co., Ltd. The remaining authors declare that the research was conducted in the absence of any commercial or financial relationships that could be construed as a potential conflict of interest.

References

1. Cheng, Y.; Yu, R.; Zhou, Q.; Chen, H.; Yuan, W.; Zhang, Y. Real-Time Sensing of Gas Metal Arc Welding Process—A Literature Review and Analysis. *J. Manuf. Process.* **2021**, *70*, 452–469. [[CrossRef](#)]
2. Xu, Y.; Liu, Q.; Xu, J.; Xiao, R.; Chen, S. Review on Multi-Information Acquisition, Defect Prediction and Quality Control of Aluminum Alloy GTAW Process. *J. Manuf. Process.* **2023**, *108*, 624–638. [[CrossRef](#)]
3. Zhang, Z.; Zhang, L.; Wen, G. Study of inner porosity detection for Al-Mg alloy in arc welding through on-line optical spectroscopy: Correlation and feature reduction. *J. Manuf. Process.* **2019**, *39*, 79–92. [[CrossRef](#)]
4. Gao, X.; Wang, L.; You, D.; Chen, Z.; Gao, P.P. Synchronized Monitoring of Droplet Transition and Keyhole Bottom in High Power Laser-MAG Hybrid Welding Process. *IEEE Sens. J.* **2019**, *19*, 3553–3563. [[CrossRef](#)]
5. Fan, X.; Gao, X.; Zhang, N.; Ye, G.; Liu, G.; Zhang, Y. Monitoring of 304 Austenitic Stainless-Steel Laser-MIG Hybrid Welding Process Based on EMD-SVM. *J. Manuf. Process.* **2022**, *73*, 736–747. [[CrossRef](#)]
6. Zhang, L.; Basantes-Defaz, A.C.; Ozevin, D.; Indacochea, E. Real-Time Monitoring of Welding Process Using Air-Coupled Ultrasonics and Acoustic Emission. *Int. J. Adv. Manuf. Technol.* **2019**, *101*, 1623–1634. [[CrossRef](#)]
7. Jin, C.; Rhee, S. Real-Time Weld Gap Monitoring and Quality Control Algorithm during Weaving Flux-Cored Arc Welding Using Deep Learning. *Metals* **2021**, *11*, 1135. [[CrossRef](#)]
8. Huang, Y.; Wu, D.; Zhang, Z.; Chen, H.; Chen, S. EMD-Based Pulsed TIG Welding Process Porosity Defect Detection and Defect Diagnosis Using GA-SVM. *J. Mater. Process. Technol.* **2017**, *239*, 92–102. [[CrossRef](#)]
9. Yu, J.; Kim, D. Effects of Welding Current and Torch Position Parameters on Minimizing the Weld Porosity of Zinc-Coated Steel. *Int. J. Adv. Manuf. Technol.* **2018**, *95*, 551–567. [[CrossRef](#)]
10. Joseph, A.; Farson, D.; Harwig, D.; Richardson, R. Influence of GMAW-P Current Waveforms on Heat Input and Weld Bead Shape. *Sci. Technol. Weld. Join.* **2005**, *10*, 311–318. [[CrossRef](#)]
11. Jin, C.; Shin, S.; Yu, J.; Rhee, S. Prediction Model for Back-Bead Monitoring During Gas Metal Arc Welding Using Supervised Deep Learning. *IEEE Access* **2020**, *8*, 224044–224058. [[CrossRef](#)]
12. Zhao, D.; Wang, Y.; Liang, D.; Ivanov, M. Performances of Regression Model and Artificial Neural Network in Monitoring Welding Quality Based on Power Signal. *J. Mater. Res. Technol.* **2020**, *9*, 1231–1240. [[CrossRef](#)]
13. Huang, Y.; Yang, D.; Wang, K.; Wang, L.; Fan, J. A Quality Diagnosis Method of GMAW Based on Improved Empirical Mode Decomposition and Extreme Learning Machine. *J. Manuf. Process.* **2020**, *54*, 120–128. [[CrossRef](#)]
14. Yu, P.; Xu, G.; Gu, X.; Zhou, G.; Tian, Y. A Low-Cost Infrared Sensing System for Monitoring the MIG Welding Process. *Int. J. Adv. Manuf. Technol.* **2017**, *92*, 4031–4038. [[CrossRef](#)]

15. Huang, N.E.; Shen, Z.; Long, S.R.; Wu, M.C.; Shih, H.H.; Zheng, Q.; Yen, N.-C.; Tung, C.C.; Liu, H.H. The Empirical Mode Decomposition and the Hilbert Spectrum for Non-linear and Non- Stationary Time Series Analysis. *Proc. Math. Phys. Eng. Sci.* **1998**, *454*, 903–995. [[CrossRef](#)]
16. Wu, Z.; Huang, N.E. Ensemble Empirical Mode Decomposition: A Noise-Assisted Data Analysis Method. *Adv. Adapt. Data Anal.* **2009**, *1*, 1–41. [[CrossRef](#)]
17. Yeh, J.-R.; Shieh, J.-S.; Huang, N.E. Complementary Ensemble Empirical Mode Decomposition: A Novel Noise Enhanced Data Analysis Method. *Adv. Adapt. Data Anal.* **2010**, *2*, 135–156. [[CrossRef](#)]
18. Imaouchen, Y.; Kedadouche, M.; Alkama, R.; Thomas, M. A Frequency-Weighted Energy Operator and Complementary Ensemble Empirical Mode Decomposition for Bearing Fault Detection. *Mech. Syst. Signal Process.* **2017**, *82*, 103–116. [[CrossRef](#)]
19. Liu, F.; Gao, J.; Liu, H. The Feature Extraction and Diagnosis of Rolling Bearing Based on CEEMD and LDWPSO-PNN. *IEEE Access* **2020**, *8*, 19810–19819. [[CrossRef](#)]
20. Gao, S.; Li, T.; Zhang, Y.; Pei, Z. Fault Diagnosis Method of Rolling Bearings Based on Adaptive Modified CEEMD and 1DCNN Model. *ISA Trans.* **2023**, *140*, 309–330. [[CrossRef](#)]
21. Zhao, L.; Yu, W.; Yan, R. Rolling Bearing Fault Diagnosis Based on CEEMD and Time Series Modeling. *Math. Probl. Eng.* **2014**, *2014*, 101867. [[CrossRef](#)]
22. Syahroni, N.; Winando, S.S.; Mulyadi, Y. Influence Analysis of Shielding Gas Flow Rate and Purity Level Variation on GMAW Welding Process to Microstructure of Alumunium 5083. *Int. J. Offshore Coast. Eng.* **2021**, *5*, 18–22. [[CrossRef](#)]

Disclaimer/Publisher’s Note: The statements, opinions and data contained in all publications are solely those of the individual author(s) and contributor(s) and not of MDPI and/or the editor(s). MDPI and/or the editor(s) disclaim responsibility for any injury to people or property resulting from any ideas, methods, instructions or products referred to in the content.